中国激光

飞秒激光成丝诱导荧光空间分布特性研究进展

薛嘉云[1,2]，齐鹏飞[1,2]，郭兰军[1,2]，张楠[1,2]，林列[1,3*]，刘伟伟[1,2]

[1]南开大学现代光学研究所，天津 300350；

[2]天津市微尺度光学信息技术科学重点实验室，天津 300350；

[3]天津市光电传感器与传感网络重点实验室，天津 300350

摘要 光丝内部的超高钳制光强可诱导大气中的原子、分子等发生隧道电离或多光子电离，并辐射指纹荧光谱。得益于其在复杂大气环境中能够远距离传输的特点，飞秒激光成丝在大气远程探测方面具有广阔的应用前景。光丝诱导物质荧光的空间分布特性与成丝过程中激光、等离子体等参数密切相关，对于理解光丝内物理过程及调控光丝、提升远程探测信噪比等具有重要意义。综述了光丝诱导荧光在侧向、背向及前向三个重要方位的空间分布的研究进展，详细讨论了基于侧向分布表征光丝内光强及等离子体分布的方法，以及实验条件对荧光空间分布的影响，并对放大自发辐射现象及前向、背向远场空间分布的研究进展进行了介绍。最后对飞秒激光成丝诱导荧光空间分布的研究趋势进行了展望。

关键词 非线性光学；激光光学；飞秒激光成丝；大气远程探测

中图分类号 O437 **文献标志码** A **DOI**：10.3788/CJL221564

1 引 言

飞秒激光脉冲短，具有很高的峰值功率，在大气中传输时，在多种非线性效应的作用下，可以克服衍射极限进行自引导传输，并伴随着等离子体通道的产生，这一过程被称为飞秒激光成丝[1-3]。飞秒激光成丝现象包含着复杂的非线性过程，如克尔效应、等离子体散焦、自相位调制、群速度色散、四波混频等。基于这些非线性效应，飞秒激光成丝在大气远程探测[3-8]、脉冲压缩[9-10]、强太赫兹波辐射[11-13]、高次谐波产生[14]等方面展现出广阔的应用前景。

飞秒激光成丝现象在固态、液态、气态中都能被观测到[2-5,7,15]。在光强钳制效应的作用下，空气中光丝内部的光强可达到 1.45×10^{14} W/cm^2[16]。在高钳制光强的作用下，大气中的原子、分子等发生隧道电离或多光子电离[17-18]，从高能态跃迁辐射出指纹荧光谱。光丝与背景能量池的能量动态交换[19]及自聚焦与等离子体散焦的动态平衡使光丝的传输距离可达到千米量级[20-21]。此外，光丝可以在复杂大气环境中进行传输，光丝中等离子体的能量可以沉积至空气中并产生冲击波，能够清除传输路径上的云雾[22-23]。面对复杂大气湍流，光丝的非线性性质，尤其是克尔效应，可以在一定程度上抑制光束的漂移[24]。因此，飞秒激光成丝在远程大气污染监测方面展现出巨大的优势。与传统雷达技术结合而形成的光丝激光雷达技术可以实现多物态、多组分同步监测，包括气体（如 N_2、O_2、CH_4、C_2H_2、氟利昂等）[25-26]，盐气溶胶（NaCl、$PbCl_2$、$CuCl_2$、$FeCl_2$等）[27-28]，金属（铅、铬、镉、铜、铝等）[29-30]以及生物成分（酵母，蛋白等）[31-32]的监测。

面向大气污染远程探测应用需求，提高探测信号的强度及信噪比对于光丝激光雷达技术发展至关重要。一方面，研究者们在实验上通过多种手段调控光丝，增强光丝与探测物质间的相互作用强度，提升远程荧光信号水平。例如，通过引入初始负啁啾来补偿大气中的色散，在传输过程中压缩激光脉冲，增强光丝内光强[33]；利用时空聚焦的方法，使不同光谱成分在空间上发生色散，在焦点处重合以增强光丝[34]；引入辅助脉冲加热分子，提高电离率并延长等离子体寿命[35]；利用相位补偿离轴系统的像散，提升远距离光丝的强度[36]。另一方面，从收集端出发，优化收集装置，也会对提高探测信噪比产生重要影响。因此，飞秒激光成丝诱导大气分子荧光的空间分布，对于研究光丝与大气分子间的作用机理，表征光丝内部参数，优化收集装置，提高远程探测的信噪比，降低污染物浓度检测限具有重要应用价值。

飞秒激光成丝诱导荧光的侧向分布被广泛用于表征光丝内激光强度、等离子体密度及温度等重要参数，相比于其他探测方法，具有非侵入、原位测量的优

收稿日期：2022-12-28；**修回日期**：2023-02-07；**录用日期**：2023-02-13；**网络首发日期**：2023-02-23

基金项目：国家重点研发计划（2018YFB0504400）、中央高校基本科研业务费（63223052）

通信作者：*linlie@nankai.edu.cn

势。利用光丝激光雷达进行远程大气污染探测时，往往采用背向收集的方式。因此光丝诱导荧光的背向分布对于优化收集效率、提高探测信噪比具有实际应用价值。前向和背向空气激光是远程遥感技术的理想光源，其远场空间分布，尤其是发散角和方向性，对于远程应用具有重要意义。本文主要从侧向、背向及前向三个重要方位，回顾了光丝诱导荧光空间分布的研究进展。重点介绍了光丝诱导荧光的侧向空间分布以及对侧向分布的调控，包括多种实验条件的影响，利用荧光侧向分布对光丝进行可视化处理，表征光丝内部光强及等离子体分布。然后对放大自发辐射现象及不同实验条件下背向、前向的远场空间分布进行了介绍。最后总结并展望了光丝诱导荧光空间分布的发展趋势。

2　飞秒激光成丝诱导荧光的侧向分布

2.1　荧光侧向分布及影响因素

由于光丝内的高钳制光强，介质发生多光子电离或隧道电离，并辐射出指纹荧光谱。荧光信号的强度可以反映光丝内光强及等离子体密度分布。因此，飞秒激光成丝诱导荧光的侧向分布是表征光丝、测量光丝内超快物理过程及调控光丝的重要参数。图 1 为不同实验条件下光丝诱导荧光的侧向分布。对于远距离光丝，可以通过飞行时间法来确定其侧向分布[17,37]。这种方法通过使用快速响应的探测器，将背向荧光传输到探测器的时间转换为传输距离，如图 1(a)所示。对于近距离产生的短光丝，也可以直接在光丝侧向利用光谱仪测量荧光信号[38]或利用电荷耦合元件(CCD)拍摄光丝[39-40]。通过测量光丝侧向荧光分布，可以对飞秒激光成丝过程进行可视化研究。研究者在实验上直接观察到了多次聚焦现象[图 1(b)][41]以及多丝的产生和竞争过程[图 1(c)～(e)][40]。

在飞秒激光成丝过程中，激光能量[42]、光斑尺寸[43]、脉宽、啁啾[33,44-45]及外部聚焦条件[6]等实验条件会直接对光丝的长度产生影响，从而影响荧光的侧向分布。除此之外，泵浦激光的偏振态也会影响光丝辐射荧光信号的长度[46]和强度[47]。由于激光偏振态对成丝的临界功率有影响[47]，圆偏振光条件下的临界功率更高，因此光丝后移，长度变短[46]。在低激光强度下，线偏光诱导的荧光信号较圆偏光更强[图 2(a)]。当激光峰值功率远高于成丝临界功率时，圆偏光诱导的荧光信号更强[图 2(b)][48]。在低激光能量下，线偏光具有更高的电离率。当能量升高后，由于圆偏光对电子的加速作用，电子具有更高的能量，通过碰撞激发产生了更多处于激发态的粒子[48-49]，从而辐射出更强的

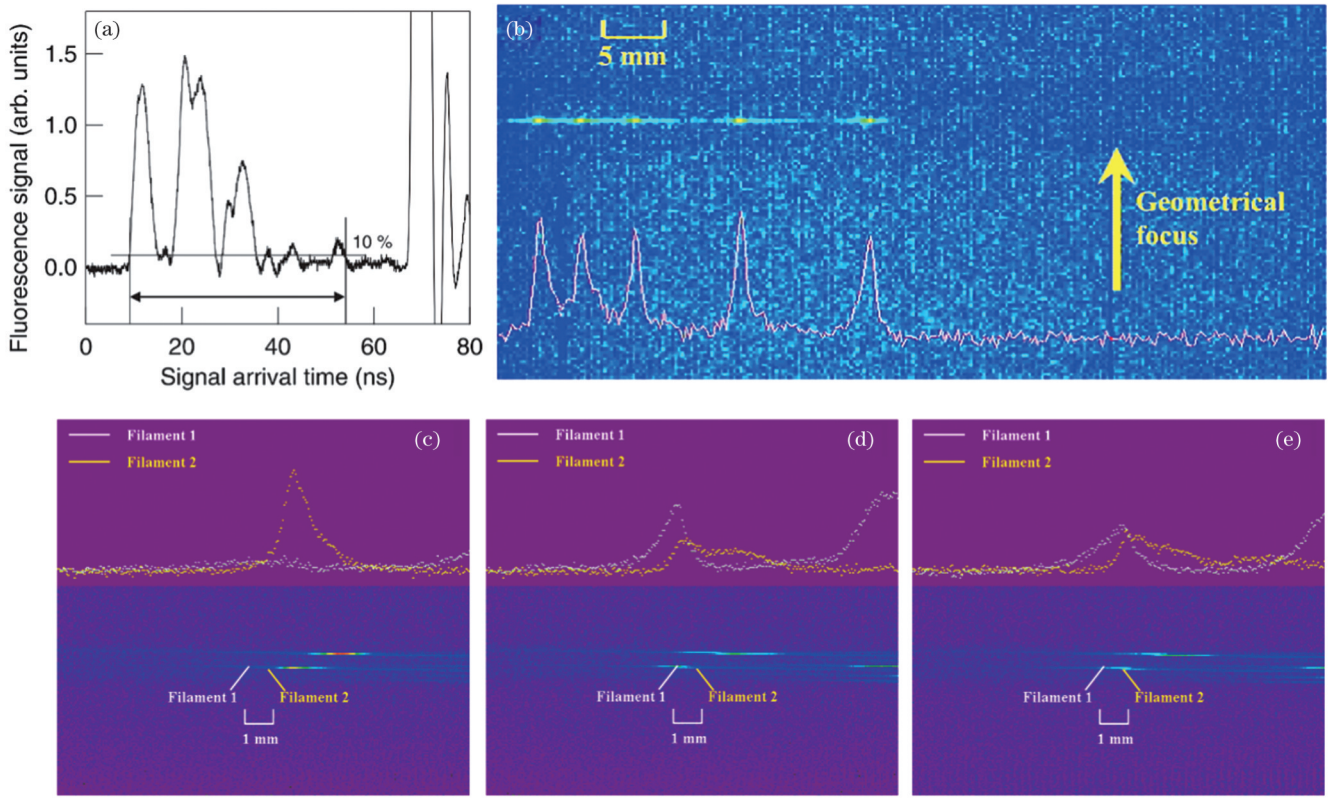

图 1　飞秒激光成丝诱导荧光的侧向空间分布。(a)利用背向荧光飞行时间法确定光丝长度[37]；(b)在溶解有染料的甲醇溶液中观测到的多次自聚焦现象[41]和(c)～(e)光丝的竞争过程[40]

Fig. 1　Lateral spatial distribution of fluorescence induced by femtosecond laser filamentation. (a) Measuring length of filament by backward-fluorescence time-of-flight method[37]; (b) multiple self-focusing phenomenon[41] and (c)-(e)competitive processes of optical filaments[40] observed in methanol solution dissolved with dyes

荧光信号。除此之外，激光的偏振态对钳制光强同样有影响[47,50]。

飞秒激光的重复频率也会影响空气中光丝辐射氮气荧光信号的强度及空间分布[图 2(c)～(d)][51]。当飞秒激光重复频率增加时，荧光信号强度反而降低，侧向分布范围呈现后移及缩小的趋势，如图 2(c)所示。理论计算表明，这一现象是光丝诱导空气热动力学过程引起的。当光丝中等离子体复合时，能量沉积到空气中并产生热扩散。当使用高重复频率的飞秒激光时，空气密度并未恢复，因而荧光信号强度降低。该结果也从侧面说明飞秒激光成丝过程中的热效应可以持续毫秒量级。

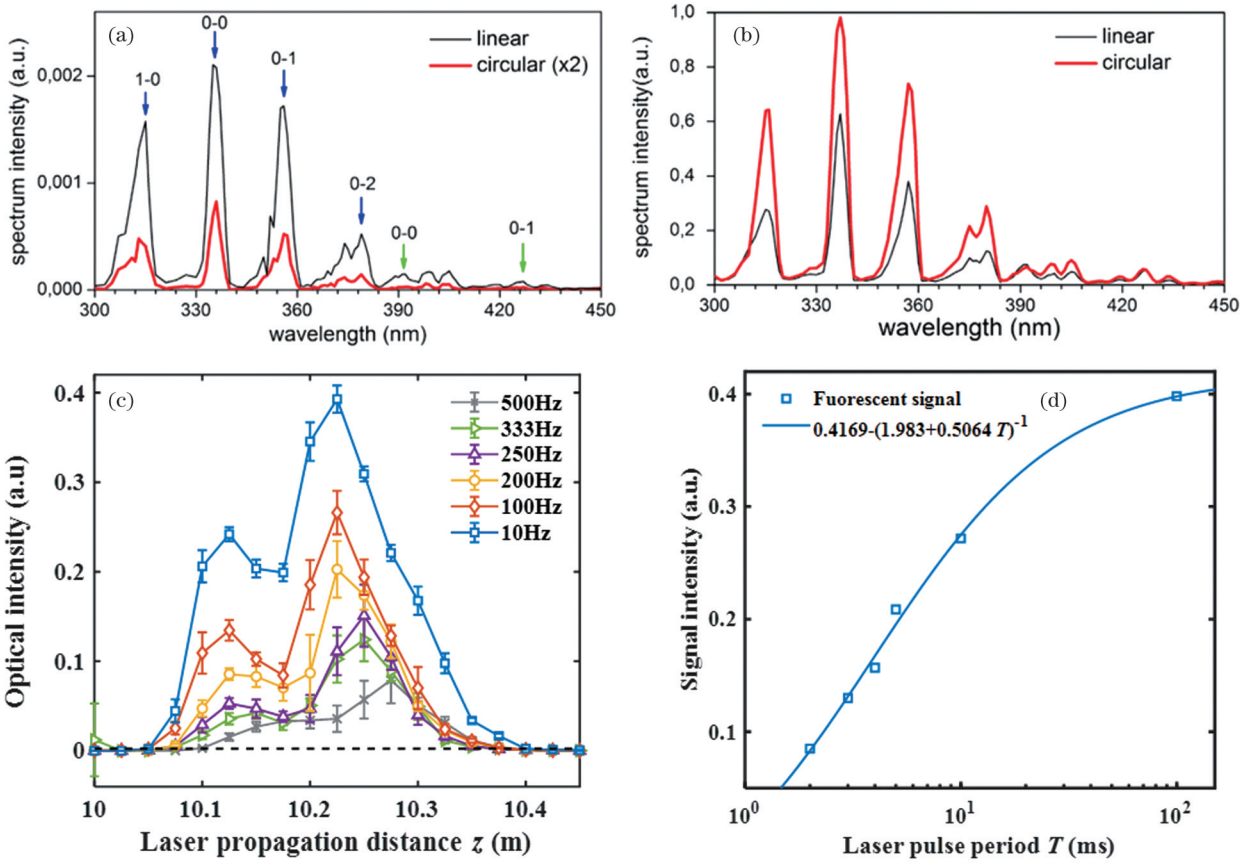

图 2　激光参数对侧向荧光空间分布的影响。激光能量为(a) 250 μJ和(b) 8.3 mJ时线偏振及圆偏振泵浦激光成丝诱导的侧向氮气荧光谱[48]；(c)不同激光重复频率下氮气荧光的侧向空间分布[51]；(d)荧光信号强度随脉冲周期变化的拟合曲线[51]

Fig. 2　Effects of laser parameters on lateral fluorescence spatial distribution. Lateral nitrogen fluorescence spectra induced by linearly and circularly polarized pumped laser filamentation at laser energies of (a) 250 μJ and (b) 8.3 mJ[48]; (c) lateral spatial distribution of nitrogen fluorescence under different laser repetition rates[51]; (d) fitting curve of fluorescence signal intensity versus pulse period[51]

在飞秒激光成丝过程中，泵浦激光会对光丝中的分子产生作用，进而对光丝长度、等离子体密度及荧光辐射强度等造成影响[52]。将这一现象应用在实验中可以提升太赫兹波的辐射效率[53]。在飞秒激光成丝过程中，强激光会诱导分子波包转动，通过引入探测光相互作用，可以实现对分子排列的调控。如图 3(a)、(b)所示，当分子排列取向垂直于探测光偏振方向时，荧光的侧向空间分布范围增大[54]。Su等[39]研究了光丝中分子排列对荧光信号方位角分布的影响，发现在偶极跃迁与分子排列的共同作用下，空气中光丝诱导的N_2^+荧光角分布具有各向异性。主要表现为在垂直和平行于激光偏振方向上氮离子荧光信号更强，如图 3(c)所示。通过计算不同分子排列情况下的荧光角分布[图 3(d)、(e)]，发现在线偏振飞秒激光的作用下，氮分子的取向最初是沿着激光的偏振方向，随后分子波包的旋转造成分子取向垂直于激光偏振方向，因而产生了各向异性的荧光角分布。

通过对侧向荧光空间分布的观测，Yu等[55]发现，在使用双色场激光成丝辐射太赫兹波的过程中，零延迟附近N_2荧光强度出现极小值，而太赫兹强度出现极大值(图 4)。主要原因是：当双色激光在零延迟附近时，电离产生的激发态N_2分子及其最高占据分子轨道(HOMO-1)所发生的电子捕获会导致等离子体密度存在最小值。并且证明了影响 THz 辐射的主要原因是光丝内双色场作用产生的电子漂移速度，而非等离子体密度。

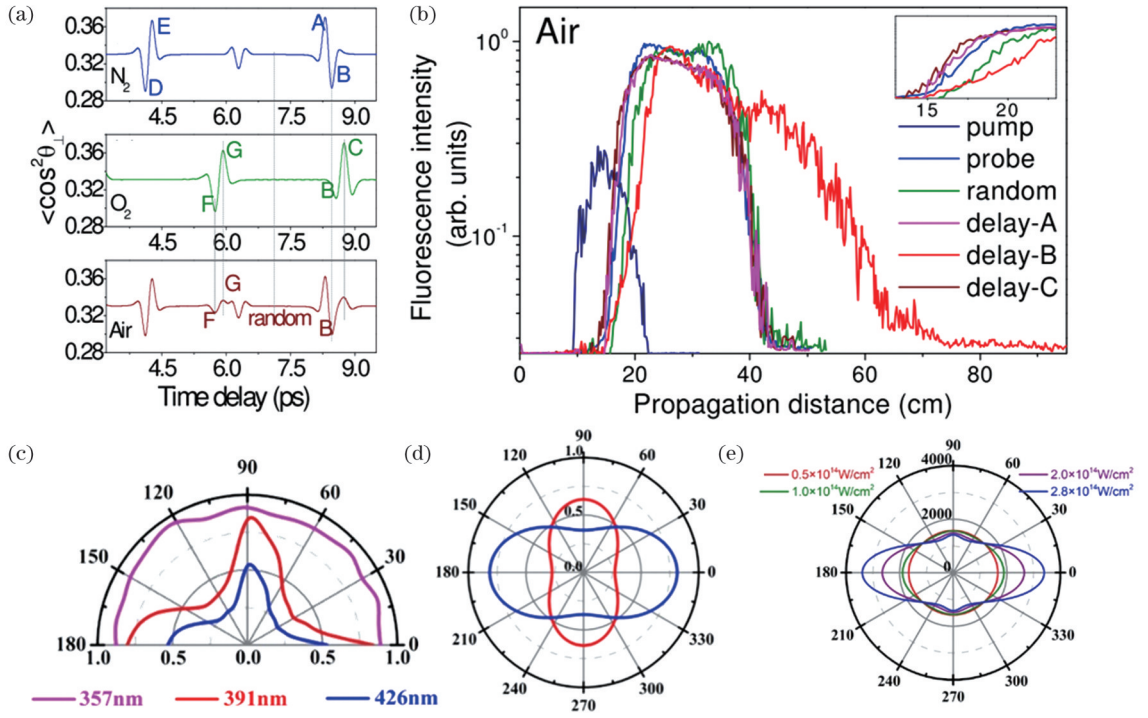

图 3　分子排列取向对光丝诱导荧光的影响。(a)N_2、O_2和空气分子的排列取向随泵浦探测光之间时间延迟的变化[54];(b)不同分子排列取向下光丝诱导荧光的侧向分布[54];(c)氮气荧光相对强度随泵浦光偏振方向的变化[39];(d)N_2分子取向平行或垂直于激光偏振方向时 391 nm 荧光信号的空间角分布[39];(e)不同激光强度下时间平均的 391 nm 荧光信号空间分布[39]

Fig. 3　Effects of molecular alignment on fluorescence induced by filament. (a) Calculated molecular alignment versus pump-probe delay in N_2, O_2, and air[54]; (b) lateral distributions of fluorescence induced by filament under different molecular alignments[54]; (c) relative intensity of nitrogen fluorescence versus polarization direction of pump light[39]; (d) spatial angular distribution of 391 nm fluorescence signal when N_2 molecule orientation is parallel or perpendicular to laser polarization direction[39]; (e) Time-averaged azimuthal distribution of 391 nm fluorescence signal under different laser intensities[39]

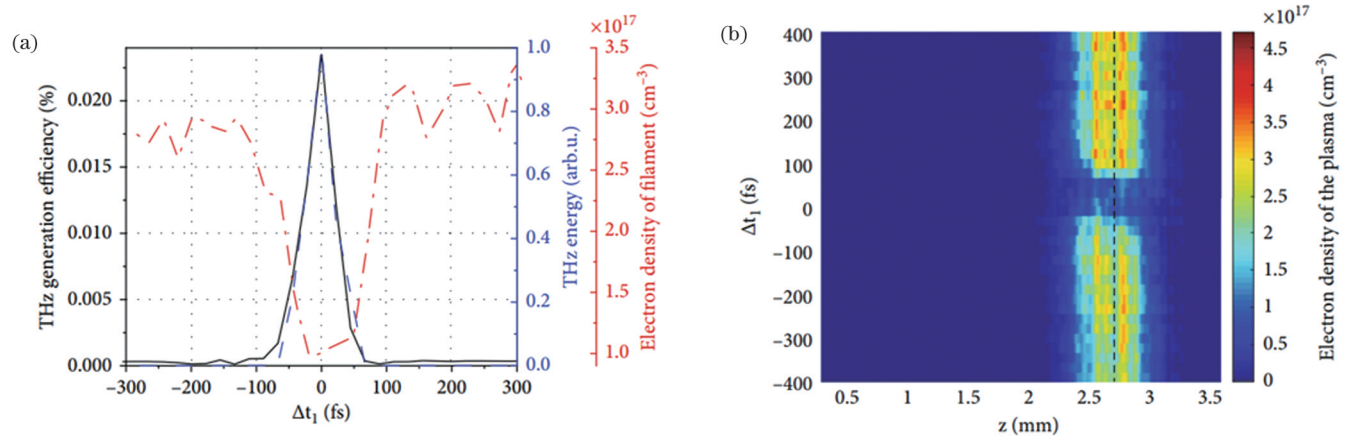

图 4　双色场成丝中呈负相关的 THz 强度与等离子体密度[55]。(a)实验与仿真得到的 THz 产生效率随双色场时间延迟的变化;(b)侧向等离子体密度分布随双色场时间延迟的变化

Fig. 4　Anti-correlated plasma density and THz intensity during two-color field filamentation[55]. (a) THz production efficiency versus time delay of two-color field obtained by experiment and simulation; (b) lateral plasma density distribution versus time delay of two-color field

2.2　基于荧光侧向分布的光丝表征

光丝内部的光强极高，在空气中可达到 5×10^{13} W/cm^2[56]，足以破坏任何探测器，无法使用侵入式的探测方法进行直接测量。而荧光辐射的产生主要是由于光丝内部发生了多光子电离或隧道电离效应[18]，因此荧光信号的强度与光丝内激光光强相关。光丝诱导荧光的侧向分布是一种被广泛用于表征光丝内部光强及长度的原位、非侵入式手段[17,42]。

氮气作为空气中的主要成分之一，常被用于研究光丝与空气的作用机制。图 5(a)、(b)所示分别为氮

分子能级图[57]和典型的氮气荧光谱，其中337、357、391、428 nm四条谱线被广泛研究。337 nm和357 nm来源于氮气分子第二正带系——从$C^3\Pi_u$态到$B^3\Pi_g$态的跃迁，391 nm和428 nm来源于氮气分子离子第一负带系——从$B^2\Sigma_u^+$态到$X^2\Sigma_g^+$态的跃迁。空气中光丝内部的激光光强可以通过391 nm与337 nm的氮气荧光信号强度比值来定量确定。由于这两条谱线分别来源于N_2^+和N_2，激发机制不同，信号强度与光强之间具有不同的非线性关系。研究者据此拟合出经验公式：

$$I_0 = 79 \times \left(\frac{2.6}{R} - 1\right)^{-0.34} \times 10^{12}, \tag{1}$$

式中：R为391 nm与337 nm氮气荧光信号的强度之比；I_0为光丝内的激光光强。只需要简单测量两条谱线的信号强度，即可得到光丝内部的激光光强，如图5(d)所示[38]。图5(d)中激光光强在光丝尾部达到2.8×10^{14} W/cm^2，远超过该聚焦条件下的钳制光强。主要原因是在空间上光丝直径减小，在时间上激光脉冲被压缩[38,58]。利用这种方法，Xu等[59]还发现，光丝内部的钳制光强受到外部聚焦条件的影响，在紧聚焦条件下(焦距f=11 cm)，空气中光丝内部的钳制光强可达到1×10^{14} W/cm^2[图5(c)]。

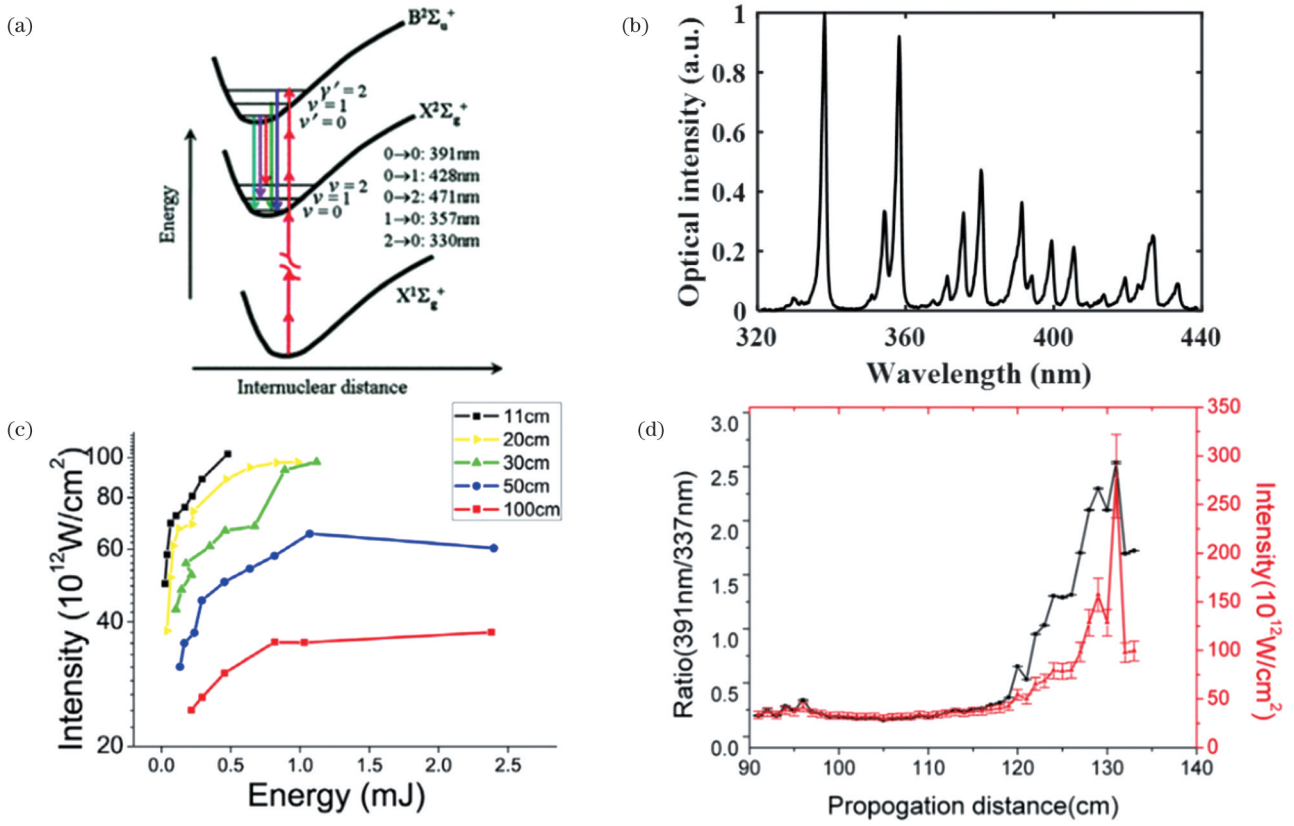

图5　利用391 nm与337 nm氮气荧光信号比值确定光丝内的激光光强。(a)氮气分子和离子能级图[57]；(b)典型的氮气荧光光谱[57]；(c)不同聚焦条件下光丝内的峰值光强随激光能量的变化[59]；(d) 391 nm与337 nm氮气荧光信号比值及光丝内的激光光强随激光传输距离的变化[38]

Fig. 5　Laser intensity inside filament deduced by ratio of 391 nm to 337 nm nitrogen fluorescence signal. (a) Energy level diagram of N_2 and N_2^+[57]; (b) typical nitrogen fluorescence spectrum[57]; (c) peak light intensity in filament versus laser energy under different focusing conditions[59]; (d) ratio of 391 nm to 337 nm nitrogen fluorescence signal and laser intensity in filament versus laser transmission distance[38]

光丝诱导荧光的侧向分布也可以用于表征光丝内部等离子体的温度及密度。光丝内部的等离子体密度及电子碰撞过程决定了其诱导荧光谱线的线宽。通过测量荧光谱线的斯塔克展宽(Stark broadening)，即可得到光丝内等离子体密度分布[60]。根据光丝辐射荧光谱的相对强度，可以由玻尔兹曼分布获得光丝内部电子的振动温度及转动温度[61-62]。对于重复频率为1 kHz、单脉冲能量为2 mJ、脉宽为42 fs、波长为800 nm的激光脉冲，在焦距为1 m的条件下，光丝内部等离子体密度可以达到5.5×10^{16} cm^{-3}，电子温度可以达到5800 K，如图6所示。相对于超声探测[63]、电导率[64]、阴影图、衍射[65]及干涉[66]等方法，利用原子荧光谱线测量等离子体密度更为简单，无需校准标定，测量灵敏度和精度更高。

2.3　光丝荧光侧向分布的调控方法

根据光丝诱导荧光的侧向空间分布，可以获得光丝内部光强及等离子体的空间分布信息。因此，实验上经常通过荧光的侧向分布判断光丝的空间位置及调

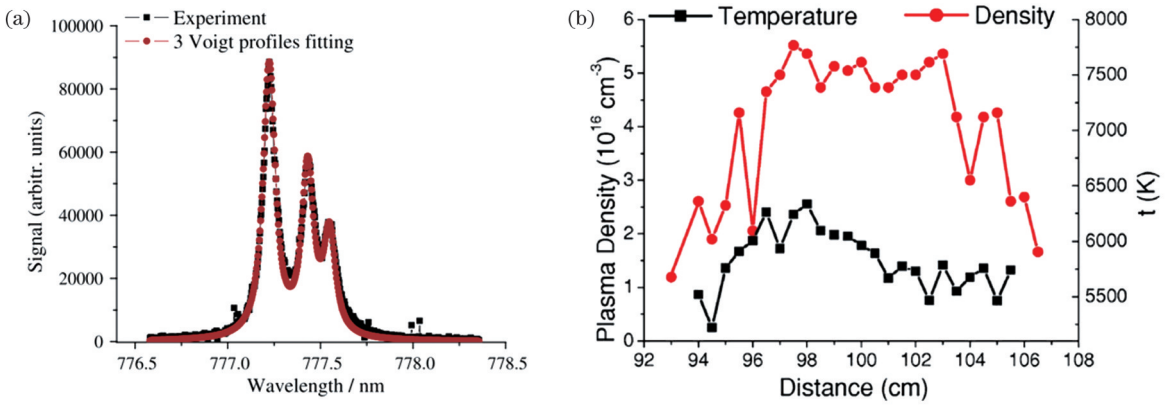

图 6　利用侧向荧光信号表征光丝等离子体密度及温度。(a)氧原子谱线[60];(b)光丝内等离子体密度及温度[61]

Fig. 6　Characterizing plasma density and temperature by lateral fluorescence signal. (a) Oxygen atomic line[60]; (b) plasma density and temperature inside filament[61]

控质量。飞秒高斯光束在介质中产生光丝时,起始位置(z_f')受到外部聚焦条件f和激光参数的影响:

$$z_f'=\frac{z_f f}{z_f+f}, \tag{2}$$

$$z_f=\frac{0.367ka^2}{\left\{\left[\left(P/P_{cr}\right)^2-0.852\right]^2-0.0219\right\}^{1/2}}, \tag{3}$$

式中:z_f为由激光参数决定的自聚焦距离;ka^2为光束的衍射长度,其中,k为激光波矢大小,a为光束束腰半径;P为激光的峰值功率;P_{cr}为自聚焦阈值功率,由介质折射率(n_0)、非线性折射率系数(n_2)和波长(λ)决定:

$$P_{cr}=\frac{3.77\lambda^2}{8\pi n_0 n_2}。 \tag{4}$$

因此,根据式(2)~(4)可知,多种实验条件会对光丝的位置及长度产生影响,包括激光能量[42]、光斑尺寸[43]、脉宽、啁啾[33,44-45]及外部聚焦条件[6]等,进而会对光丝诱导荧光的侧向空间分布产生影响。

考虑到在外部聚焦条件下,飞秒激光成丝之前非线性效应引起的自聚焦效应可以忽略,同时将激光峰值强度导致空气电离的位置作为成丝起点,本课题组推导出一个简单的物理公式[33],可以定量解释实验结果,有效估算光丝的起始点位置(z_{th})和长度,即

$$z_{th}=\sqrt{\frac{\alpha E_{in}}{\sqrt{1+\left(C+C_0\right)^2}}}-\beta, \tag{5}$$

式中:$\alpha=(2\pi)^{1/2}a^2/(\lambda^2 I_{th}\tau_0)$,其中,$I_{th}$为电离空气的阈值激光光强,$\tau_0$为傅里叶变换极限脉宽;$\beta$为衍射长度的平方;$E_{in}$为入射激光能量;$C$和$C_0$分别为由光栅对和群速度色散引起的啁啾系数。理论上,光丝的长度为起始位置至几何焦距的距离。通过改变激光啁啾,可以延长或缩短光丝,即调控荧光侧向分布范围[33,44-45]。

相比于时间啁啾调控方法,时空聚焦方法是一种更为有效的方法,可以同时起到调节侧向分布范围及荧光信号强度的作用[34,67],如图 7(a)所示。利用光栅产生空间色散,使不同光谱成分的光只在焦点处重合,激光脉冲被压缩,从而光丝内的峰值光强得到提升。利用这种方法形成的光丝长度更短,在远程探测中具有更高的空间分辨率,同时,光丝诱导的荧光信号更

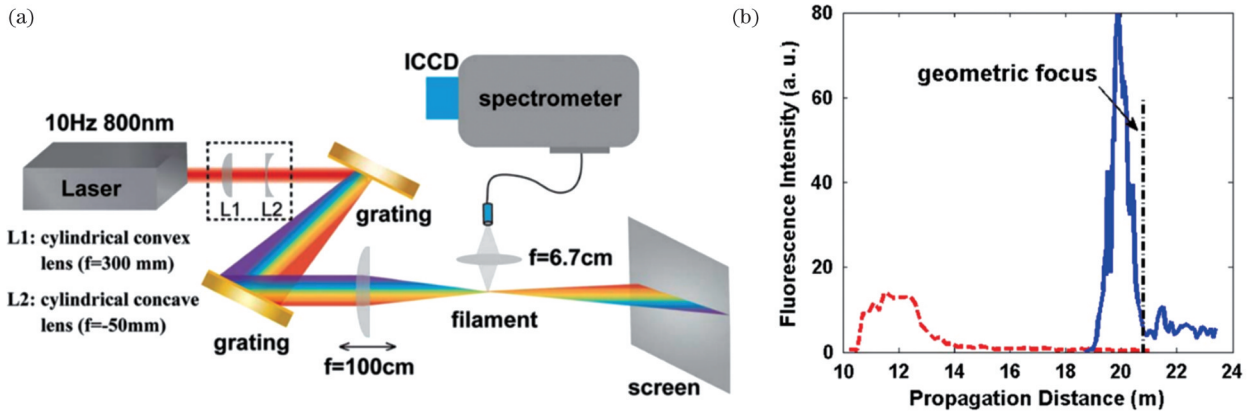

图 7　通过时空聚焦调控光丝[34]。(a)时空聚焦实验装置示意图;(b)时空啁啾(实线)与无啁啾(虚线)两种情况下的 337 nm 荧光信号的侧向空间分布

Fig. 7　Regulating filament by spatiotemporal focusing[34]. (a) Schematic of spatiotemporal focusing experimental device; (b) lateral spatial distributions of 337 nm fluorescence signal with (solid line) and without (dotted line) chirp

强，如图 7(b)所示。

延长光丝对于飞秒激光成丝在远程遥感、大气污染探测、导引微波传输、引雷等方面的应用具有重要价值。通过提高初始激光能量，可以延长光丝[68]。但当能量过高时，会形成多丝。研究者尝试通过多种时空相位调控的方法延长光丝，如控制双脉冲之间的时间延迟[69]，使用轴锥镜聚焦产生贝塞尔光束[70]，使用空间光调制器加载多焦点相位[71]，使用相位板加载阶梯形π相位[72]等。背景能量池与光丝之间能量的动态交换在维持光丝长距离传输时起到重要作用[19]。如图 8(a)、(b)所示，研究者提出通过空间光调制器产生环形光束，中心的高斯光束聚焦形成光丝，周围的环状结构形成背景能量池，不断补充光丝的能量，从而达到延长光丝的目的[73]。延长光丝后，光丝内荧光信号可经历更长的增益长度[74]，从而提高远程探测的信噪比。如图 8(c)所示，利用空间色散和时间啁啾之间的耦合，使不同波长的光聚焦在不同的空间位置处，激光脉冲传输距离达近 100 倍的瑞利长度并且不发散[75]。除了对侧向分布范围的调控，Polynkin 等[76]通过调控光束相位，利用艾里光束改变了光丝传播方向，产生了弯曲的光丝，如图 8(d)、(e)所示，从而在前向产生了可区分的锥角辐射。

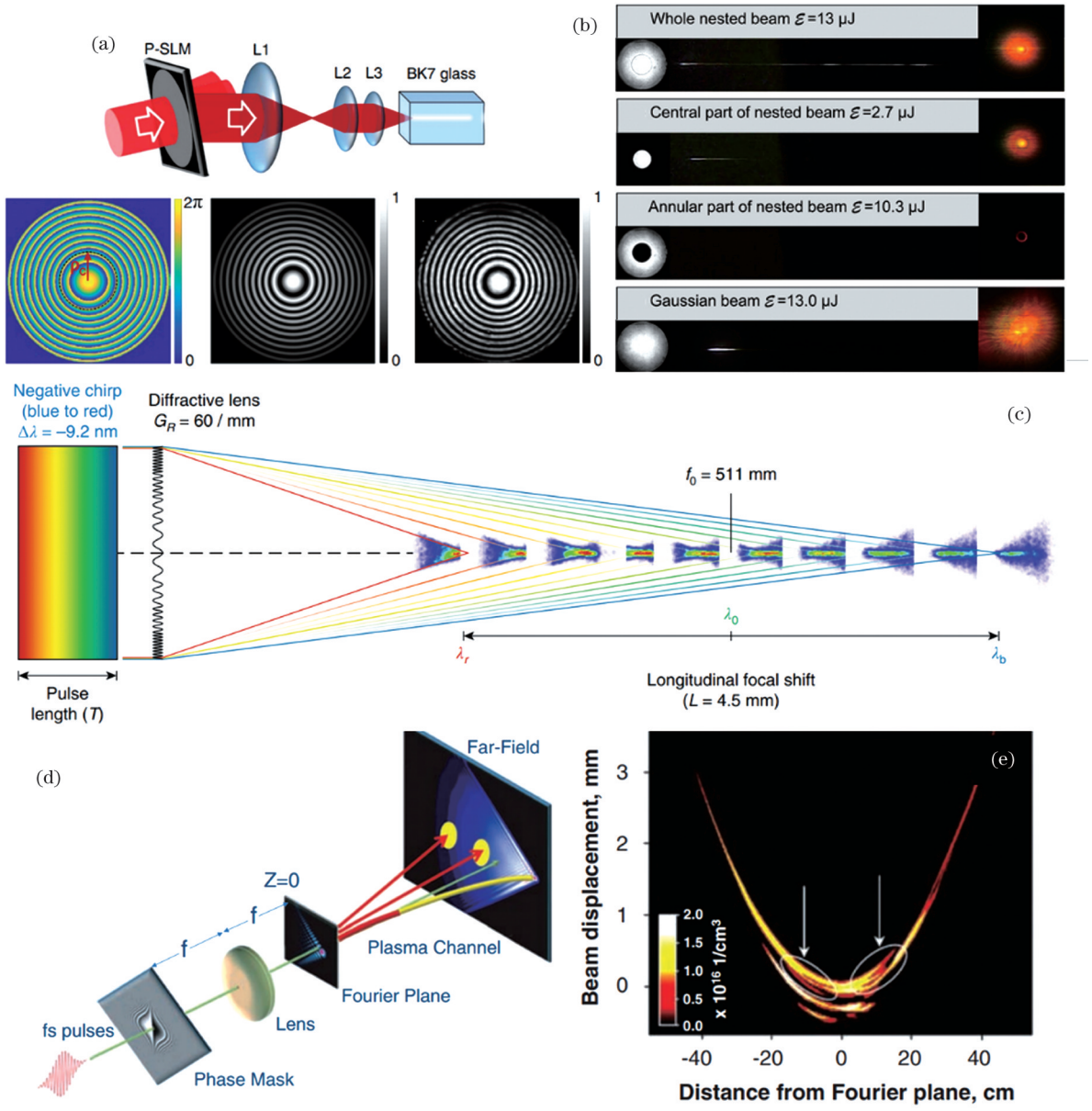

图 8　时空相位整形延长光丝。(a)产生环形光束的实验装置示意图[73]；(b)不同光束成丝情况对比[73]；(c)空间色散与时间啁啾耦合实验装置示意图[75]；(d)产生弯曲光丝实验装置示意图[76]；(e)弯曲光丝的侧向空间分布[76]

Fig. 8　Lengthening filament by spatiotemporal phase shaping. (a) Schematic of experimental setup for generating ring beam[73]; (b) comparison of filament induced by different beams[73]; (c) diagram of experimental setup for coupling spatial dispersion and time chirp[75]; (d) schematic of experimental setup for generating curved filament[76]; (e) lateral spatial distribution of curved filament[76]

由于实验中使用的激光光斑模式并不完全理想，或者环境中存在湍流等扰动，当峰值功率过高时，经常会产生多丝。多丝的调控也属于侧向空间分布的调控，主要包括两个方面：抑制多丝产生和有序调控多丝。控制热点之间的距离，比如使用望远镜系统进行缩束[43]，可以有效抑制多丝的产生。实验上通过使用轴锥镜[68]、相位板[72]、空间光调制器[77]等调制激光光束的相位，减少热点周围的能量，同样可以达到抑制多丝产生的目的，并在一定程度上增大其侧向分布范围，并提高光丝诱导荧光信号的稳定性[43,78]。另一方面，有序产生的光丝阵列可推动光丝直写波导[79]、微波波导[80]及太赫兹产生[81]等方面的应用。如图 9 所示，通过使用轴锥镜[68]、透镜阵列[82-83]、相位板[84-85]、变形镜[86]、金属网筛[87]及改变光束的椭圆度[88-89]等，控制热点的产生并增加背景能量池之间的距离，可以在侧向有序产生多根光丝。

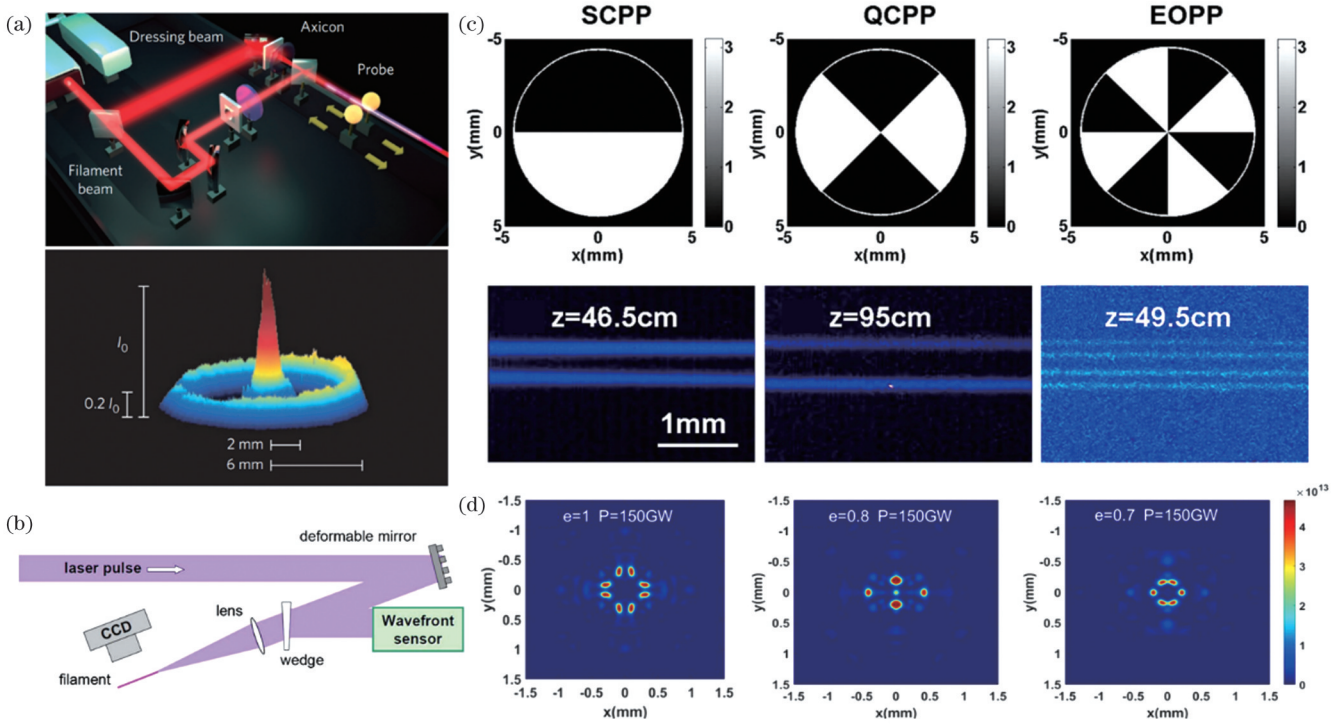

图 9　使用不同方法调控多丝。(a)使用辅助光束[90]；(b)使用变形镜[86]；(c)使用相位板及其产生的多丝[85]；(d)改变光束椭圆度[88]

Fig. 9　Controlling multiple filaments by different methods. (a) Using auxiliary beam[90]; (b) using deformable mirror[86]; (c) using phase plates and generated multiple filaments[85]; (d) changing beam ellipticity[88]

3　飞秒激光成丝诱导荧光的背向分布

在大气远程探测技术中，常采用背向探测的方式。因此背向光信号的激发机制、空间分布及传输特性对于远程信号收集具有重要意义。对于非相干光辐射，其传输方向具有随机性，因此背向信号收集端只能收集到少部分光信号。如果远程产生的光信号具有方向性，远程探测的灵敏度将会提升[91]，同时空气激光的发现也为大气遥感提供了新的技术思路。

空气激光无需光学谐振腔，可凭借光丝的特性在远距离处产生，具有良好的方向性，已成为远场产生新激光源的重要方式。2003 年，研究者首次发现了光丝中氮气荧光的放大自发辐射(ASE)现象，随后以光丝作为增益介质产生空气激光的物理机制与调控方法得到广泛研究。

光丝中的 ASE 现象主要表现为背向荧光信号强度随光丝长度呈指数增长，如图 10 所示。Luo 等[74,92]在实验上证明了光丝内氮气荧光信号存在增益。引起这种现象的主要原因是：在等离子体的复合及弛豫过程中，氮分子从更高能级跃迁至 $C^3\Pi_u$ 能级，而 $B^3\Pi_g$ 仍然是空的，因而在 $C^3\Pi_u$ 和 $B^3\Pi_g$ 能级之间形成了粒子数反转[74]。利用背向荧光信号强度与光丝长度的指数拟合，可以得到不同物质荧光的增益系数，大多在 0.5 cm^{-1} 量级。目前，实验上能观测到空气中多种物质成分的放大自发辐射现象，包括氮气分子[74]以及 CN[93]、OH[94]、NH[95]、CH 化合物[96]，如图 10 所示。2011 年，研究者利用紫外泵浦光产生了背向传输的具有高增益和高方向性的近红外氧原子激光，发光波长为 845 nm，增益系数可以高达 62 cm^{-1}，空间分布呈环状结构[图 11(a)]，发散角为 40 mrad。氧原子激光的激发机制可以总结为：波长为 226 nm 的紫外激光通过受激双光子共振解离氧分子，并通过双光子共振将氧原子激发至高能态，随后辐射出波长为 845 nm 的氧原子激光。利用另一束激光预先解离氧分子，可以在背向实现更高的增益效果[91]。

除了上述提到的利用等离子体弛豫过程[74]及双光

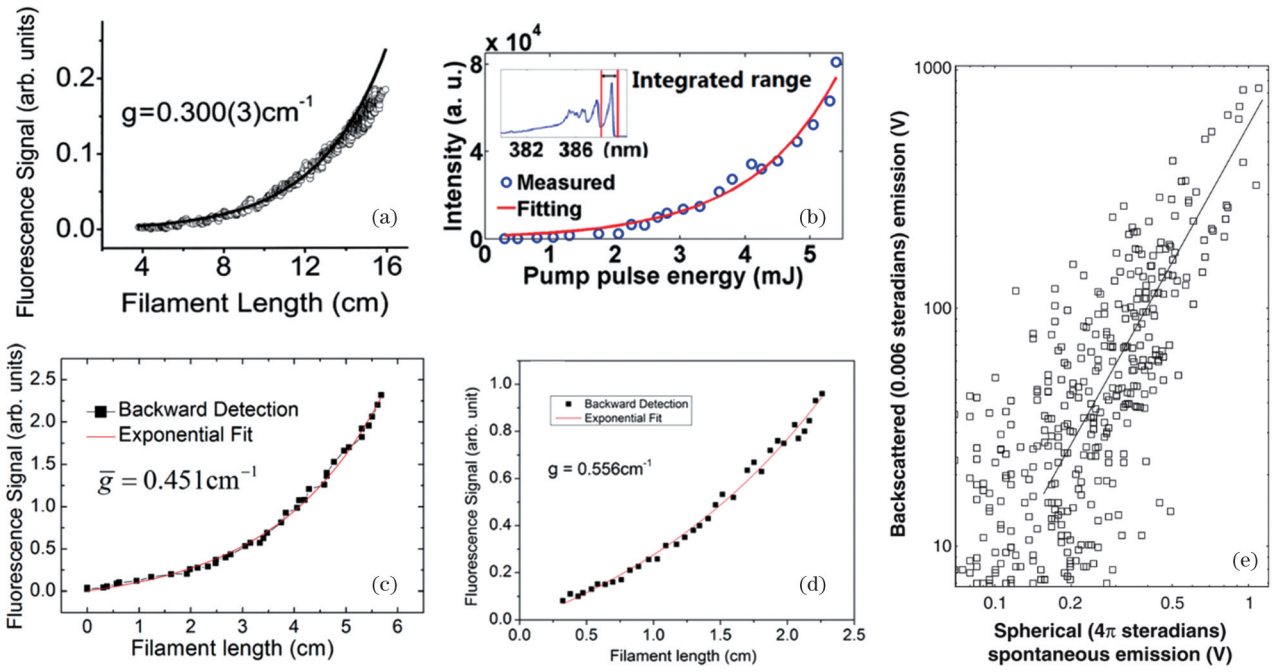

图 10　背向 ASE 荧光增益曲线。(a)波长为 357 nm 的氮分子荧光[74]；(b)波长为 388 nm 的 CN 荧光[93]；(c)波长为 308.9 nm 的 OH 荧光[94]；(d)波长为 336 nm 的 NH 荧光[95]；(e)波长为 845 nm 的氧原子荧光[91]

Fig. 10　Gain curves of backward ASE fluorescence. (a) N_2 fluorescence at 357 nm[74]; (b) CN fluorescence at 388 nm[93]; (c) OH fluorescence at 308.9 nm[94]; (d)NH fluorescence at 336 nm[95]; (e) oxygen atom fluorescence at 845 nm[91]

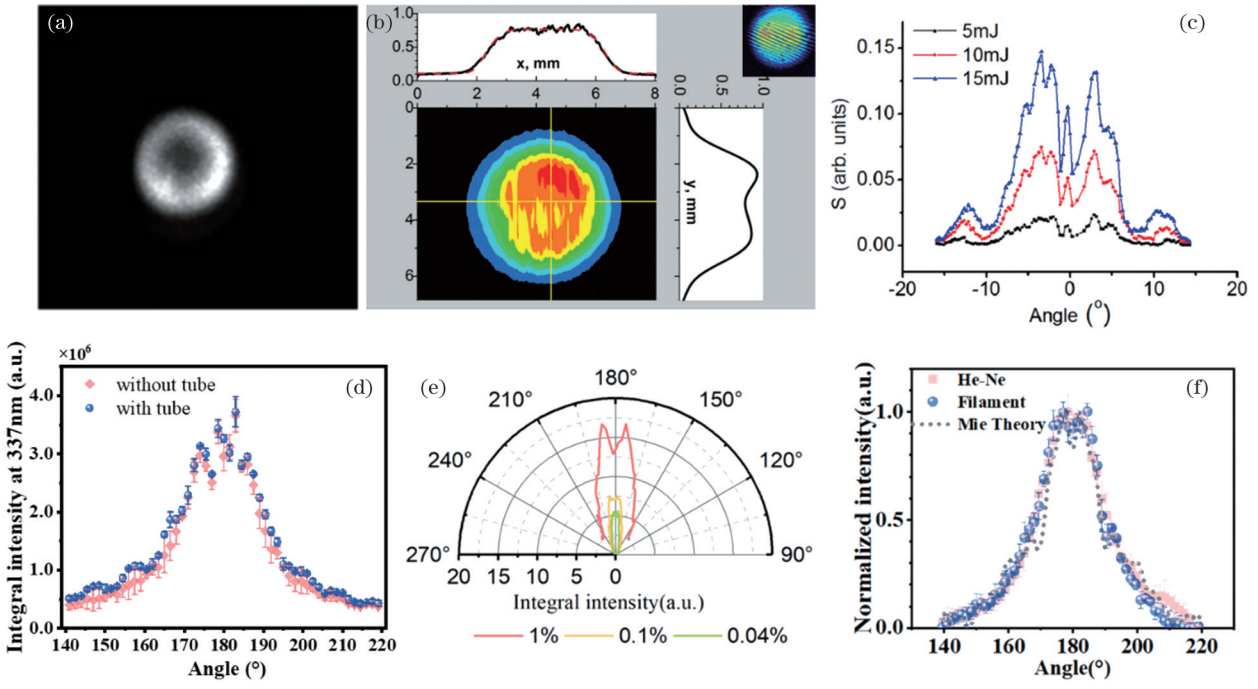

图 11　背向荧光的空间分布。(a) 845 nm 背向氧原子激光的空间分布[91]；(b)通过氩原子碰撞激发产生的氮分子激光的空间分布[97]；(c) 357 nm 氮气荧光信号的背向角分布，输入能量分别为 5、10、15 mJ[100]；(d)光丝诱导 337 nm 氮气荧光的背向角分布[101]；(e)不同浓度 NaCl 气溶胶中 589 nm 钠荧光的背向角分布[101]；(f)NaCl 气溶胶荧光背向角分布与米散射信号强度角分布的对比[101]

Fig. 11　Spatial distributions of backward fluorescence. (a) Spatial distribution of backward oxygen atom laser at 845 nm[91]; (b) spatial distribution of nitrogen laser generated by argon collision excitation[97]; (c) backward angular distributions of 357 nm nitrogen fluorescence signal with input energies of 5, 10, and 15 mJ[100]; (d) backward angular distributions of 337 nm nitrogen fluorescence induced by filament[101]; (e) backward angular distribution of sodium fluorescence at 589 nm in NaCl aerosols with different mass fractions[101]; (f) comparison of backward angular distribution of NaCl aerosol fluorescence and angular distribution of Mie scattering signal intensity[101]

子激发[91]产生粒子数反转的方法外，还可以利用碰撞激发能量共振转移[97]产生粒子数反转。研究者利用中红外激光(3.9 μm)成丝过程产生激发态氩原子[98]，其与氮气分子发生碰撞，通过能量共振转移产生激发态氮分子($C^3\Pi_u$)，从而形成粒子数反转，辐射出 337 nm 与 357 nm 的氮分子激光[97]。利用这种方式产生的氮分子激光具有良好的时间相干性及较小的空间发散角。图 11(b)为氮分子激光的背向空间分布情况，光斑呈超高斯分布，发散角约为 1.6 mrad。但这种碰撞过程会受到气压的影响，无法在远程探测中应用。Sprangle 等[99]还提出在成丝过程中引入一束辅助脉冲，加热成丝产生的自由电子，然后通过电子碰撞产生激发态粒子，从而实现更高的增益。

光丝诱导荧光的背向空间分布，尤其是角分布，对于远程信号探测中收集装置的视场角及尺寸的设计具有重要意义。研究者在实验上发现 ASE 现象具有角度依赖的性质。在外部聚焦条件为 1 m 的情况下，如图 11(c)所示，探测到背向氮气荧光(357 nm)信号主要集中在光轴附近 ±10°发散角范围内，发散角为 46 mrad。此外，在不同角度下观测到的荧光信号强度具有不同的增益系数，主要是光丝内部非均匀分布的等离子体密度造成的。等离子体密度越高，增益系数越大，产生的荧光信号越强[100]。通过对传输距离为 10 m、长度为 50 cm 的光丝所诱导的荧光信号进行测量，研究者发现氮气荧光信号(337 nm)具有与图 11(c)相似的背向分布情况，集中在传输轴附近 ±10°范围内[101]，如图 11(d)所示。由于飞秒激光成丝在远程大气污染探测方面的优势，光丝诱导的气溶胶荧光信号的背向角分布也得到深入研究。如图 11(e)、(f)所示，NaCl 气溶胶荧光信号具有对称的角分布，且受到气溶胶浓度的影响，浓度越高，背向发散角越大，在 NaCl 质量分数为 1% 的情况下，发散角为 14.4°。理论模拟计算米散射的角分布，并将结果与 He-Ne 激光经气溶胶散射后的角分布情况进行对比，发现造成气溶胶背向荧光角分布的主要原因是米散射[101]。

背向空气激光的信号强度还受到泵浦激光偏振态的影响，且这种偏振敏感的性质在泵浦激光能量改变时，具有完全不同的表现[48-49]。如图 12(a)、(b)所示，

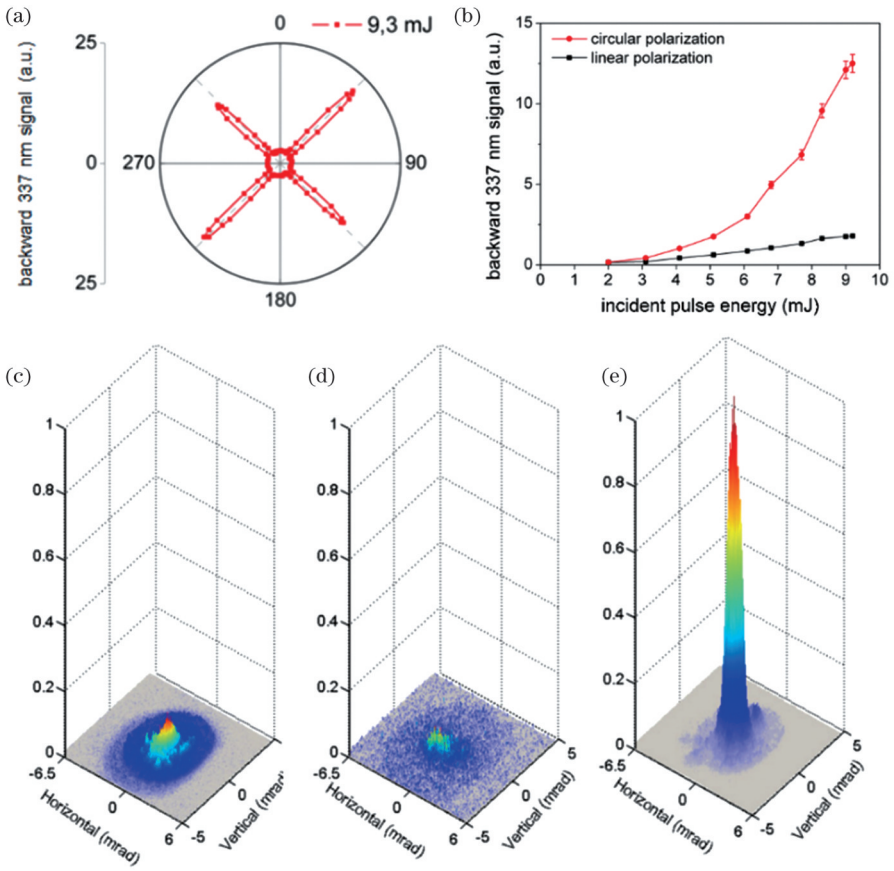

图 12　偏振依赖的背向 337 nm 荧光信号。(a)背向 337 nm 荧光信号随四分之一波片旋转角度的变化[49]；(b)背向 337 nm 荧光信号在不同激光偏振条件下随入射激光能量的变化[49]；(c)种子光的空间分布[102]；(d)ASE 背向 337 nm 荧光信号的空间分布[102]；(e)种子光放大产生的 337 nm 光信号的空间分布[102]

Fig. 12　Polarization-dependence backward fluorescence signal at 337 nm. (a) Change of fluorescence signal at 337 nm with rotation angle of quarter-wave plate[49]; (b) backward fluorescence at 337 nm versus incident laser energy under different laser polarization conditions[49]; (c) spatial distribution of seed pulse[102]; (d) spatial distribution of backward ASE fluorescence signal at 337 nm[102]; (e) spatial distribution of 337 nm optical signal generated by seed optical amplification[102]

0°和45°分别代表线偏振光和圆偏振光。只有激光光强达到阈值时，圆偏振泵浦光激发的氮分子荧光信号才会强于线偏振泵浦光所激发的荧光信号。原因是当激光光强较低时，虽然会产生碰撞过程，但电子能量不足以将分子激发至高能态。通过引入一束与圆偏振泵浦光相向传输的种子光[图 12(c)]，ASE信号受激放大，背向荧光的发散角进一步减小，如图 12(d)、(e)所示。受激放大的荧光信号的背向发散角为 3.8 mrad[图 12(e)]，而未经放大的ASE信号，其背向发散角为 9.2 mrad[图 12(d)][102]。

4　飞秒激光成丝诱导荧光的前向分布

利用光丝产生的粒子数反转，引入种子光，光丝作为增益介质可产生前向的受激辐射。种子光可以是外加的激光光束[103]，也可以是光丝自身丰富的非线性光频转换效应辐射出的谐波或超连续白光[104-105]。

Yao等[57]使用波长可调谐的中红外光学参量放大器（波长范围为 1600～2500 nm，其中 1900 nm 波长下测得的激光脉宽为 200 fs）作为泵浦光，以空气中激发产生的三次、五次谐波作为种子光，实现了多波长的氮离子激光输出[图 13(a)]，波长分别为 330、357、391、428、471 nm。其中，波长为 391 nm 的氮离子激光具有与泵浦激光相同的偏振特性，且增益系数可以达到 5.02 cm^{-1}，远大于空气中 ASE 现象的增益系数[图 13(b)]。多波长可调谐空气激光在大气多组分检测中起到重要作用。

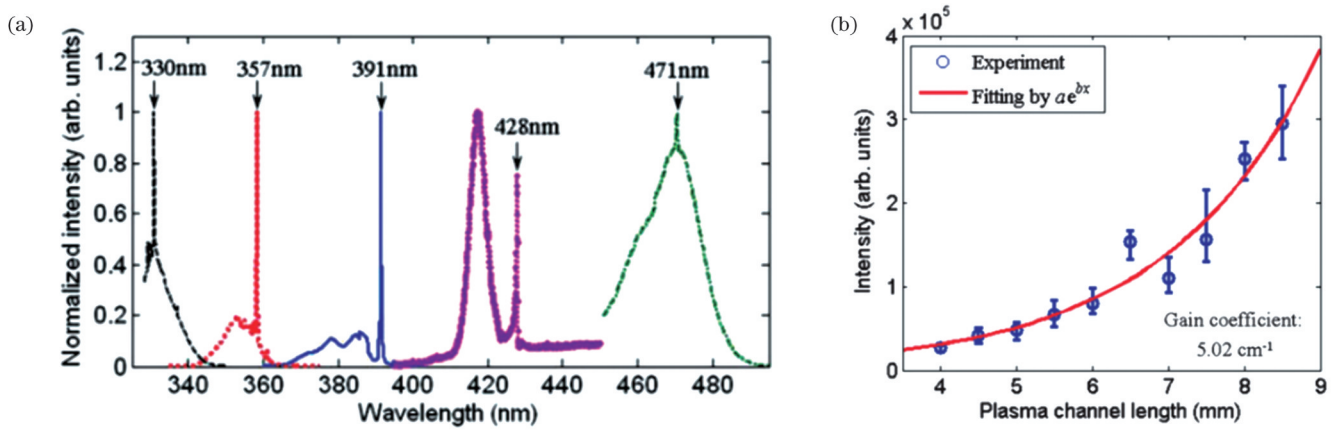

图 13　前向空气激光及其偏振特性[57]。(a)利用不同波长泵浦光产生的可调谐多波长空气激光；(b) 391 nm空气激光的增益曲线

Fig. 13　Forward air laser and its polarization characteristics[57]. (a) Tunable multi-wavelength air laser generated by pumping light with different wavelengths; (b) gain curve of 391 nm air laser

上述实验中利用飞秒激光产生了氮离子激光（$B^2\Sigma_u^+ \rightarrow X^2\Sigma_g^+$），而未产生波长为 337 nm 的氮分子激光（$C^3\Pi_u \rightarrow B^3\Pi_g$）。该现象产生的主要原因是：氮离子激光是飞秒激光作为泵浦光激发产生的。因为只需要电离内价层和外价层的电子，N_2^+ 的 $B^2\Sigma_u^+$ 和 $X^2\Sigma_g^+$ 两个能级之间的粒子数反转过程属于超快过程（～200 fs），而产生 $C^3\Pi_u$ 态的氮分子则需要皮秒量级的时间[57,106-107]。随后，研究者以波长为 1053 nm 的皮秒激光产生的三次谐波作为种子光，激发产生了前向的氮分子激光（337 nm）[108]。在峰值功率为 1 TW 的情况下，脉宽的增加对前向 337 nm 信号的产生具有增强作用。因为氮分子的粒子数反转过程需要皮秒量级的时间，而脉宽较短的激光脉冲无法在粒子数反转产生的同时保证三次谐波依然存在并作为种子光产生受激辐射放大。利用这种方式产生的 337 nm 信号，空间发散角为 1.5°[图 14(a)]，且能量在微焦量级，转化效率为 2.5×10^{-7} [108]。

飞秒激光成丝诱导的前向空气激光的空间分布特性也引起了广泛关注。如图 14(b)所示，Chu等[104]利用飞秒激光成丝过程中产生的超连续白光作为种子源，激发产生的 428 nm 氮离子激光在远场呈环状分布。Kartashov等[109]利用 4 μm 波长的中红外激光激发产生的前向 337 nm 氮分子激光，同样具有相似的环状结构[图 14(c)]。Liu等[105]发现，气压对前向空气激光的空间分布及强度具有重要影响。他们利用自激发的方式产生了前向的氮离子激光，波长为 391 nm 和 428 nm。如图 14(d)所示，当气压增大时，391 nm 信号的发散角变大，在原来高斯分布的基础上呈现出外环结构。在图 14(e)中，波长为 428 nm 的空气激光呈环状分布[104-105]，发散角达到 20 mrad[105]，且具有与泵浦激光相同的线偏振特性[104]。研究者认为，428 nm 激光是超连续白光作为种子光激发产生的，因此其环状分布源于超连续辐射锥形分布。此外，数值模拟结果同样显示，前向传输的空气激光具有环状分布结构，如图 14(f)所示。外部聚焦条件和克尔效应对前向激光的信号强度和发散角具有重要影响，如图 14(g)所示。同时，在远程应用中，克尔效应对维持空气激光的方向性具有重要作用[110]。

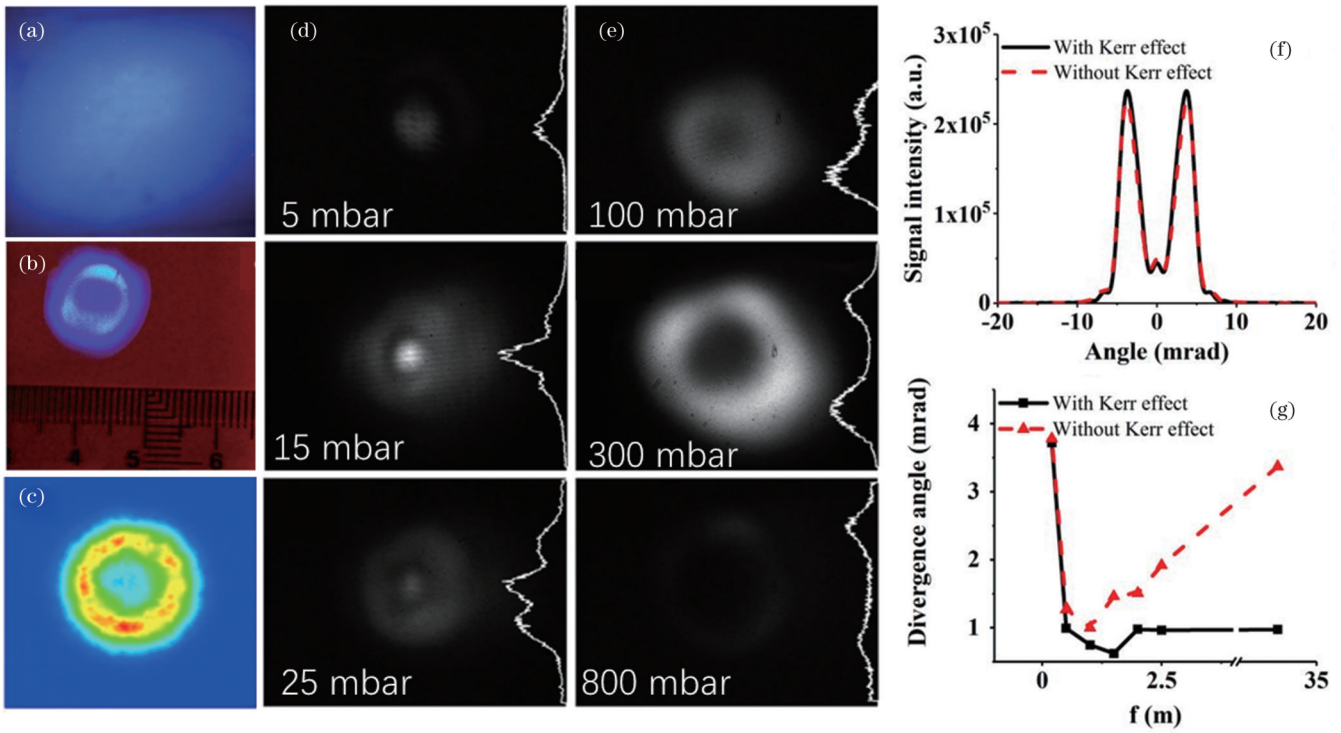

图 14　前向空气激光的远场空间分布。(a)皮秒激光三次谐波激发产生的 337 nm 空气激光的远场分布[108]；(b)光丝诱导白光自激发的 428 nm 空气激光的远场分布[104]；(c) 3.9 μm 中红外激光激发的 337 nm 空气激光的远场空间分布[109]；(d)不同气压下光丝自激发的 391 nm 空气激光的空间分布[105]；(e)不同气压下光丝自激发的 428 nm 空气激光的远场空间分布[105]；(f)数值模拟的 337 nm 空气激光的远场角分布[110]；(g)空气激光发散角随外部聚焦条件的变化[110]

Fig. 14　Far-field spatial distributions of forward air laser. (a) Far-field distribution of 337 nm air laser generated by third harmonic excitation of picosecond laser[108]; (b) far-field distribution of 428 nm air laser self-excited by filament-induced white light[104]; (c) far-field spatial distribution of 337 nm air laser excited by 3.9 μm mid-infrared laser[109]; (d) spatial distributions of 391 nm air laser self-excited by filament under different atmospheric pressures[105]; (e) far-field spatial distributions of 428 nm air laser self-excited by filament under different atmospheric pressures[105]; (f) simulated far-field angular distribution of air laser at 391 nm[110]; (g) divergence angle of air laser versus external focusing condition [110]

5　总结与展望

光丝诱导荧光空间分布的研究对于理解光丝内物理化学机制、调控光丝、产生空气激光及大气远程探测等具有重要的价值。从侧向、背向及前向三个重要空间方位介绍了荧光空间分布的研究进展，包括实验条件的影响、表征和调控光丝、放大自发辐射现象及背向和前向远场空间分布。目前，飞秒激光成丝诱导荧光技术在大气污染探测方面的应用仍存在一些重要挑战。首先，光丝与大气中各种分子、粉尘及气溶胶等相互作用、激发荧光的物理机制复杂，仍然需要深入探究。光丝中的增益现象广泛存在于氮气、氧气、碳氢化合物及多种气溶胶中，且基于粒子数反转、碰撞激发、种子光激发、多态耦合等效应产生了多种空气激光。空气激光增益放大的物理机制研究在远程大气污染探测中具有重要价值。其次，在实际应用中，复杂的大气环境，包括湍流、大气温湿度分布、气压分布、大气散射与吸收等多物理场耦合对荧光空间分布的影响机制尚未明晰。最后，调控光丝中光强的时空分布是增强荧光信号的关键，如何通过调控产生远程、高品质的光丝，并提升远程探测的信噪比，降低污染物的探测极限，仍然需要广大科研人员深入研究。

参　考　文　献

[1] Braun A, Korn G, Liu X, et al. Self-channeling of high-peak-power femtosecond laser pulses in air[J]. Optics Letters, 1995, 20(1): 73-75.

[2] 刘伟伟，薛嘉云，苏强，等. 超快激光成丝现象研究综述[J]. 中国激光，2020，47(5)：0500003.
Liu W W, Xue J Y, Su Q, et al. Research progress on ultrafast laser filamentation[J]. Chinese Journal of Lasers, 2020, 47(5): 0500003.

[3] Qi P F, Qian W Q, Guo L J, et al. Sensing with femtosecond laser filamentation[J]. Sensors, 2022, 22(18): 7076.

[4] Xu H L, Chin S L. Femtosecond laser filamentation for atmospheric sensing[J]. Sensors, 2011, 11(1): 32-53.

[5] Luo Q, Xu H L, Hosseini S A, et al. Remote sensing of pollutants using femtosecond laser pulse fluorescence spectroscopy [J]. Applied Physics B, 2006, 82(1): 105-109.

[6] Liu W, Théberge F, Daigle J-F, et al. An efficient control of ultrashort laser filament location in air for the purpose of remote sensing[J]. Applied Physics B, 2006, 85(1): 55-58.

[7] Chin S L, Xu H L, Luo Q, et al. Filamentation “remote” sensing of chemical and biological agents/pollutants using only one femtosecond laser source[J]. Applied Physics B, 2009, 95(1): 1-12.

[8] Xu H L, Cheng Y, Chin S L, et al. Femtosecond laser ionization

and fragmentation of molecules for environmental sensing[J]. Laser & Photonics Reviews, 2015, 9(3): 275-293.

[9] Stibenz G, Zhavoronkov N, Steinmeyer G. Self-compression of millijoule pulses to 7.8 fs duration in a white-light filament[J]. Optics Letters, 2006, 31(2): 274-276.

[10] Silva F, Austin D R, Thai A, et al. Multi-octave supercontinuum generation from mid-infrared filamentation in a bulk crystal[J]. Nature Communications, 2012, 3(1): 1-5.

[11] Yu Z Q, Zhang N, Wang J X, et al. 0.35% THz pulse conversion efficiency achieved by Ti: sapphire femtosecond laser filamentation in argon at 1 kHz repetition rate[J]. Opto-Electronic Advances, 2022, 5(9): 210065.

[12] Fedorov V Y, Tzortzakis S. Powerful terahertz waves from long-wavelength infrared laser filaments[J]. Light: Science & Applications, 2020, 9(1): 1-16.

[13] Koulouklidis A D, Gollner C, Shumakova V, et al. Observation of extremely efficient terahertz generation from mid-infrared two-color laser filaments[J]. Nature Communications, 2020, 11(1): 292.

[14] Dharmadhikari A K, Edward S, Dharmadhikari J A, et al. On the generation of polarization-dependent supercontinuum and third harmonic in air[J]. Journal of Physics B: Atomic, Molecular and Optical Physics, 2015, 48(9): 094012.

[15] Kosareva O G, Kandidov V P, Brodeur A, et al. From filamentation in condensed media to filamentation in gases[J]. Journal of Nonlinear Optical Physics & Materials, 1997, 6(4): 485-494.

[16] Mitryukovskiy S I, Liu Y, Houard A, et al. Re-evaluation of the peak intensity inside a femtosecond laser filament in air[J]. Journal of Physics B: Atomic, Molecular and Optical Physics, 2015, 48(9): 094003.

[17] Hosseini S A, Yu J, Luo Q, et al. Multi-parameter characterization of the longitudinal plasma profile of a filament: a comparative study[J]. Applied Physics B, 2004, 79(4): 519-523.

[18] Talebpour A, Yang J, Chin S L. Semi-empirical model for the rate of tunnel ionization of N_2 and O_2 molecule in an intense Ti: sapphire laser pulse[J]. Optics Communications, 1999, 163(1/2/3): 29-32.

[19] Liu W, Théberge F, Arévalo E, et al. Experiment and simulations on the energy reservoir effect in femtosecond light filaments[J]. Optics Letters, 2005, 30(19): 2602-2604.

[20] Rodriguez M, Bourayou R, Méjean G, et al. Kilometer-range nonlinear propagation of femtosecond laser pulses[J]. Physical Review E, 2004, 69(3): 036607.

[21] Dicaire I, Jukna V, Praz C, et al. Spaceborne laser filamentation for atmospheric remote sensing[J]. Laser & Photonics Reviews, 2016, 10(3): 481-493.

[22] de la Cruz L, Schubert E, Mongin D, et al. High repetition rate ultrashort laser cuts a path through fog[J]. Applied Physics Letters, 2016, 109(25): 251105.

[23] Courvoisier F, Boutou V, Kasparian J, et al. Ultraintense light filaments transmitted through clouds[J]. Applied Physics Letters, 2003, 83(2): 213-215.

[24] Guo J W, Sun L, Liu J P, et al. Beam wander restrained by nonlinearity of femtosecond laser filament in air[J]. Sensors, 2022, 22(13): 4995.

[25] Xu H L, Kamali Y, Marceau C, et al. Simultaneous detection and identification of multigas pollutants using filament-induced nonlinear spectroscopy[J]. Applied Physics Letters, 2007, 90(10): 101106.

[26] Gravel J F, Luo Q, Boudreau D, et al. Sensing of halocarbons using femtosecond laser-induced fluorescence[J]. Analytical Chemistry, 2004, 76(16): 4799-4805.

[27] Daigle J F, Méjean G, Liu W, et al. Long range trace detection in aqueous aerosol using remote filament-induced breakdown spectroscopy[J]. Applied Physics B, 2007, 87(4): 749-754.

[28] Daigle J F, Mathieu P, Roy G, et al. Multi-constituents detection in contaminated aerosol clouds using remote-filament-induced breakdown spectroscopy[J]. Optics Communications, 2007, 278(1): 147-152.

[29] Stelmaszczyk K, Rohwetter P, Méjean G, et al. Long-distance remote laser-induced breakdown spectroscopy using filamentation in air[J]. Applied Physics Letters, 2004, 85(18): 3977-3979.

[30] Liu W, Xu H L, Méjean G, et al. Efficient non-gated remote filament-induced breakdown spectroscopy of metallic sample[J]. Spectrochimica Acta Part B: Atomic Spectroscopy, 2007, 62(1): 76-81.

[31] Xu H L, Méjean G, Liu W, et al. Remote detection of similar biological materials using femtosecond filament-induced breakdown spectroscopy[J]. Applied Physics B, 2007, 87(1): 151-156.

[32] Xu H L, Liu W, Chin S L. Remote time-resolved filament-induced breakdown spectroscopy of biological materials[J]. Optics Letters, 2006, 31(10): 1540-1542.

[33] Shang B P, Qi P F, Guo J W, et al. Manipulation of Long-Distance femtosecond laser Filamentation: from physical model to acoustic diagnosis[J]. Optics & Laser Technology, 2023, 157: 108636.

[34] Zeng B, Wang T J, Hosseini S, et al. Enhanced remote filament-induced breakdown spectroscopy with spatio-temporally chirped pulses[J]. Journal of the Optical Society of America B, 2012, 29(12): 3226-3230.

[35] Chu W, Zeng B, Li Z T, et al. Range extension in laser-induced breakdown spectroscopy using femtosecond - nanosecond dual-beam laser system[J]. Applied Physics B, 2017, 123(6): 173.

[36] Tao S S, Xie B F, Xue J Y, et al. Giant enhancement of acoustic and fluorescence emission from an off-axis reflective femtosecond laser filamentation system[J]. Optics Express, 2022, 30(21): 38745-38752.

[37] Iwasaki A, Aközbek N, Ferland B, et al. A LIDAR technique to measure the filament length generated by a high-peak power femtosecond laser pulse in air[J]. Applied Physics B, 2003, 76(3): 231-236.

[38] Sun X D, Xu S Q, Zhao J Y, et al. Impressive laser intensity increase at the trailing stage of femtosecond laser filamentation in air[J]. Optics Express, 2012, 20(4): 4790-4795.

[39] Su Q, Sun L, Chu C Y, et al. Effect of molecular orbital angular momentum on the spatial distribution of fluorescence during femtosecond laser filamentation in air[J]. The Journal of Physical Chemistry Letters, 2020, 11(3): 730-734.

[40] Qi P F, Lin L, Su Q, et al. *In-situ* visualization of multiple filament competition dynamic during nonlinear propagation of femtosecond laser[J]. Scientific Reports, 2017, 7(1): 10384.

[41] Liu W, Chin S L, Kosareva O G, et al. Multiple refocusing of a femtosecond laser pulse in a dispersive liquid (methanol)[J]. Optics Communications, 2003, 225(1/2/3): 193-209.

[42] Talebpour A, Petit S, Chin S L. Re-focusing during the propagation of a focused femtosecond Ti: Sapphire laser pulse in air [J]. Optics Communications, 1999, 171(4/5/6): 285-290.

[43] Luo Q, Hosseini S A, Liu W, et al. Effect of beam diameter on the propagation of intense femtosecond laser pulses[J]. Applied Physics B, 2005, 80(1): 35-38.

[44] Liang H, Sun H Y, Liu Y H, et al. Chirp control of femtosecond laser-filamentation-induced snow formation in a cloud chamber[J]. Chinese Optics Letters, 2015, 13(3): 033201.

[45] Shumakova V, Ališauskas S, Malevich P, et al. Chirp-controlled filamentation and formation of light bullets in the mid-IR[J]. Optics Letters, 2019, 44(9): 2173-2176.

[46] Zhu Z B, Wang T J, Liu Y X, et al. Polarization-dependent femtosecond laser filamentation in air[J]. Chinese Optics Letters, 2018, 16(7): 073201.

[47] Liu C, Zang H W, Li H L, et al. Polarization effect on critical power and luminescence in an air filament[J]. Chinese Optics Letters, 2017, 15(12): 120201.

[48] Mitryukovskiy S, Liu Y, Ding P J, et al. Plasma luminescence from femtosecond filaments in air: evidence for impact excitation

with circularly polarized light pulses[J]. Physical Review Letters, 2015, 114(6): 063003.
[49] Mitryukovskiy S, Liu Y, Ding P J, et al. Backward stimulated radiation from filaments in nitrogen gas and air pumped by circularly polarized 800 nm femtosecond laser pulses[J]. Optics Express, 2014, 22(11): 12750-12759.
[50] Guo H, Dong X, Wang T J, et al. Polarization dependent clamping intensity inside a femtosecond filament in air[J]. Chinese Optics Letters, 2021, 19(10): 103201.
[51] Xue J Y, Zhang N, Guo L J, et al. Effect of laser repetition rate on the fluorescence characteristic of a long-distance femtosecond laser filament[J]. Optics Letters, 2022, 47(21): 5676-5679.
[52] Chin S L, Wang T J, Marceau C, et al. Advances in intense femtosecond laser filamentation in air[J]. Laser Physics, 2012, 22(1): 1-53.
[53] You Y S, Oh T I, Fallahkhair A B, et al. Alignment-dependent terahertz radiation in two-color photoionization of molecules[J]. Physical Review A, 2013, 87(3): 035401.
[54] Cai H, Wu J, Li H, et al. Elongation of femtosecond filament by molecular alignment in air[J]. Optics Express, 2009, 17(23): 21060-21065.
[55] Yu Z Q, Sun L, Zhang N, et al. Anti-correlated plasma and THz pulse generation during two-color laser filamentation in air[J]. Ultrafast Science, 2022, 2022: 1-7.
[56] Kasparian J, Sauerbrey R, Chin S L. The critical laser intensity of self-guided light filaments in air[J]. Applied Physics B, 2000, 71(6): 877-879.
[57] Yao J P, Zeng B, Xu H L, et al. High-brightness switchable multiwavelength remote laser in air[J]. Physical Review A, 2011, 84(5): 051802.
[58] Gaarde M B, Couairon A. Intensity spikes in laser filamentation: diagnostics and application[J]. Physical Review Letters, 2009, 103(4): 043901.
[59] Xu S Q, Sun X D, Zeng B, et al. Simple method of measuring laser peak intensity inside femtosecond laser filament in air[J]. Optics Express, 2012, 20(1): 299-307.
[60] Bernhardt J, Liu W, Théberge F, et al. Spectroscopic analysis of femtosecond laser plasma filament in air[J]. Optics Communications, 2008, 281(5): 1268-1274.
[61] Liu W, Bernhardt J, Théberge F, et al. Spectroscopic characterization of femtosecond laser filament in argon gas[J]. Journal of Applied Physics, 2007, 102(3): 033111.
[62] Owada S, Azarm A, Hosseini S, et al. Amplified spontaneous $C^3\Pi_u - B^3\Pi_g$ emission and rotational and vibrational state distributions in $C^3\Pi_u$ state of N_2 in femtosecond laser induced filament in air[J]. Chemical Physics Letters, 2013, 581: 21-25.
[63] Yu J, Mondelain D, Kasparian J, et al. Sonographic probing of laser filaments in air[J]. Applied Optics, 2003, 42(36): 7117-7120.
[64] Schillinger H, Sauerbrey R. Electrical conductivity of long plasma channels in air generated by self-guided femtosecond laser pulses[J]. Applied Physics B, 1999, 68(4): 753-756.
[65] Liu J S, Duan Z L, Zeng Z N, et al. Time-resolved investigation of low-density plasma channels produced by a kilohertz femtosecond laser in air[J]. Physical Review E, 2005, 72(2): 026412.
[66] Yang H, Zhang J, Li Y J, et al. Characteristics of self-guided laser plasma channels generated by femtosecond laser pulses in air[J]. Physical Review E, 2002, 66(1): 016406.
[67] Zeng B, Chu W, Gao H, et al. Enhancement of peak intensity in a filament core with spatiotemporally focused femtosecond laser pulses[J]. Physical Review A, 2011, 84(6): 063819.
[68] Sun X D, Zeng T, Gao H, et al. Power dependent filamentation of a femtosecond laser pulse in air by focusing with an axicon[J]. Journal of Physics B, 2015, 48(9): 094004.
[69] Tzortzakis S, Méchain G, Patalano G, et al. Concatenation of plasma filaments created in air by femtosecond infrared laser pulses[J]. Applied Physics B, 2003, 76(5): 609-612.
[70] Polynkin P, Kolesik M, Roberts A, et al. Generation of extended plasma channels in air using femtosecond Bessel beams[J]. Optics Express, 2008, 16(20): 15733-15740.
[71] Hong Z F, Zhang Q B, Ali Rezvani S, et al. Extending plasma channel of filamentation with a multi-focal-length beam[J]. Optics Express, 2016, 24(4): 4029-4041.
[72] Fu Y X, Xiong H, Xu H, et al. Generation of extended filaments of femtosecond pulses in air by use of a single-step phase plate[J]. Optics Letters, 2009, 34(23): 3752-3754.
[73] Lü J Q, Li P P, Wang D, et al. Extending optical filaments with phase-nested laser beams[J]. Photonics Research, 2018, 6(12): 1130-1136.
[74] Luo Q, Liu W, Chin S L. Lasing action in air induced by ultrafast laser filamentation[J]. Applied Physics B, 2003, 76(3): 337-340.
[75] Froula D H, Turnbull D, Davies A S, et al. Spatiotemporal control of laser intensity[J]. Nature Photonics, 2018, 12(5): 262-265.
[76] Polynkin P, Kolesik M, Moloney J V, et al. Curved plasma channel generation using ultraintense Airy beams[J]. Science, 2009, 324(5924): 229-232.
[77] Walter D, Bürsing H, Ebert R. Emission of spiral patterns from filaments in the infrared[J]. Optics Express, 2010, 18(23): 24258-24263.
[78] Hosseini S A, Luo Q, Ferland B, et al. Competition of multiple filaments during the propagation of intense femtosecond laser pulses[J]. Physical Review A, 2004, 70(3): 033802.
[79] Davis K M, Miura K, Sugimoto N, et al. Writing waveguides in glass with a femtosecond laser[J]. Optics Letters, 1996, 21(21): 1729-1731.
[80] Châteauneuf M, Payeur S, Dubois J, et al. Microwave guiding in air by a cylindrical filament array waveguide[J]. Applied Physics Letters, 2008, 92(9): 091104.
[81] Zhao J Y, Guo L J, Chu W, et al. Simple method to enhance terahertz radiation from femtosecond laser filament array with a step phase plate[J]. Optics Letters, 2015, 40(16): 3838-3841.
[82] Camino A, Hao Z Q, Liu X, et al. High spectral power femtosecond supercontinuum source by use of microlens array[J]. Optics Letters, 2014, 39(4): 747-750.
[83] Panov N A, Kosareva O G, Murtazin I N. Ordered filaments of a femtosecond pulse in the volume of a transparent medium[J]. Journal of Optical Technology, 2006, 73(11): 778-785.
[84] Liu L, Wang C, Cheng Y, et al. Fine control of multiple femtosecond filamentation using a combination of phase plates[J]. Journal of Physics B: Atomic, Molecular and Optical Physics, 2011, 44(21): 215404.
[85] Gao H, Chu W, Yu G L, et al. Femtosecond laser filament array generated with step phase plate in air[J]. Optics Express, 2013, 21(4): 4612-4622.
[86] Ionin A A, Iroshnikov N G, Kosareva O G, et al. Filamentation of femtosecond laser pulses governed by variable wavefront distortions via a deformable mirror[J]. Journal of the Optical Society of America B, 2013, 30(8): 2257-2262.
[87] Liu J S, Schroeder H, Chin S L, et al. Ultrafast control of multiple filamentation by ultrafast laser pulses[J]. Applied Physics Letters, 2005, 87(16): 161105.
[88] Liu J P, Tian X Q, Chu C Y, et al. Effect of beam ellipticity on femtosecond laser multi-filamentation regulated by π-phase plate[J]. Laser Physics Letters, 2020, 17(8): 085402.
[89] Dubietis A, Tamosauskas G, Fibich G, et al. Multiple filamentation induced by input-beam ellipticity[J]. Optics Letters, 2004, 29(10): 1126-1128.
[90] Scheller M, Mills M S, Miri M A, et al. Externally refuelled optical filaments[J]. Nature Photonics, 2014, 8(4): 297-301.
[91] Dogariu A, Michael J B, Scully M O, et al. High-gain backward lasing in air[J]. Science, 2011, 331(6016): 442-445.
[92] Luo Q, Hosseini A, Liu W W, et al. Lasing action in air induced by ultrafast laser filamentation[J]. Optics and Photonics News,

2004, 15(9): 44-47.
[93] Chu W, Li H L, Ni J L, et al. Lasing action induced by femtosecond laser filamentation in ethanol flame for combustion diagnosis[J]. Applied Physics Letters, 2014, 104(9): 091106.
[94] Yuan S, Wang T J, Teranishi Y, et al. Lasing action in water vapor induced by ultrashort laser filamentation[J]. Applied Physics Letters, 2013, 102(22): 224102.
[95] Yuan S, Wang T J, Lu P F, et al. Humidity measurement in air using filament-induced nitrogen monohydride fluorescence spectroscopy[J]. Applied Physics Letters, 2014, 104(9): 091113.
[96] Hosseini S, Azarm A, Daigle J F, et al. Filament-induced amplified spontaneous emission in air - hydrocarbons gas mixture [J]. Optics Communications, 2014, 316: 61-66.
[97] Kartashov D, Ališauskas S, Andriukaitis G, et al. Free-space nitrogen gas laser driven by a femtosecond filament[J]. Physical Review A, 2012, 86(3): 033831.
[98] Shneider M N, Baltuška A, Zheltikov A M. Population inversion of molecular nitrogen in an Ar: N_2 mixture by selective resonance-enhanced multiphoton ionization[J]. Journal of Applied Physics, 2011, 110(8): 083112.
[99] Sprangle P, Peñano J, Hafizi B, et al. Remotely induced atmospheric lasing[J]. Applied Physics Letters, 2011, 98(21): 211102.
[100] Zeng T, Zhao J Y, Liu W, et al. Backward angular distribution of air lasing induced by femtosecond laser filamentation[J]. Laser Physics Letters, 2014, 11(7): 075401.
[101] Xue J Y, Zeng X, Guo L J, et al. High directional aerosol fluorescence distribution affected by Mie scattering during femtosecond laser filamentation in air[J]. Optics & Laser Technology, 2023, 161: 109175.
[102] Ding P J, Mitryukovskiy S, Houard A, et al. Backward Lasing of Air plasma pumped by Circularly polarized femtosecond pulses for the saKe of remote sensing (BLACK)[J]. Optics Express, 2014, 22 (24): 29964-29977.
[103] Ni J L, Chu W, Jing C R, et al. Identification of the physical mechanism of generation of coherent N_2^+ emissions in air by femtosecond laser excitation[J]. Optics Express, 2013, 21(7): 8746-8752.
[104] Chu W, Li G H, Xie H Q, et al. A self-induced white light seeding laser in a femtosecond laser filament[J]. Laser Physics Letters, 2014, 11(1): 015301.
[105] Liu Y, Brelet Y, Point G, et al. Self-seeded lasing in ionized air pumped by 800 nm femtosecond laser pulses[J]. Optics Express, 2013, 21(19): 22791-22798.
[106] Danylo R, Zhang X, Fan Z Q, et al. Formation dynamics of excited neutral nitrogen molecules inside femtosecond laser filaments[J]. Physical Review Letters, 2019, 123(24): 243203.
[107] Xu H L, Azarm A, Bernhardt J, et al. The mechanism of nitrogen fluorescence inside a femtosecond laser filament in air[J]. Chemical Physics, 2009, 360(1/2/3): 171-175.
[108] Kartashov D, Ališauskas S, Baltuška A, et al. Remotely pumped stimulated emission at 337 nm in atmospheric nitrogen[J]. Physical Review A, 2013, 88(4): 041805.
[109] Kartashov D, Ališauskas S, Pugžlys A, et al. Theory of a filament initiated nitrogen laser[J]. Journal of Physics B: Atomic, Molecular and Optical Physics, 2015, 48(9): 094016.
[110] Xue J Y, Gao H, Zhang N, et al. External focusing dependence of spatial distribution of air lasers during femtosecond laser filamentation in air[J]. Chinese Optics Letters, 2021, 19(8): 081402.

Research Progress on Spatial Distribution of Fluorescence Induced by Femtosecond Laser Filamentation

Xue Jiayun[1,2], Qi Pengfei[1,2], Guo Lanjun[1,2], Zhang Nan[1,2], Lin Lie[1,3*], Liu Weiwei[1,2]

[1]*Institute of Modern Optics, Nankai University, Tianjin* 300350, *China*;
[2]*Tianjin Key Laboratory of Micro-scale Optical Information Science and Technology, Tianjin* 300350, *China*;
[3]*Tianjin Key Laboratory of Optoelectronic Sensor and Sensing Network Technology, Tianjin* 300350, *China*

Abstract

Significance The high clamping laser intensity inside the filament can ionize molecules and fragment them into plasma because of multiphoton ionization or tunneling ionization. Filamentation occurs in solids, liquids, and gases. The dynamic energy exchange between the filament core and background energy reservoir, as well as the dynamic balance of self-focusing and defocusing propagate filaments over hundreds of kilometers. Nevertheless, filaments can also overcome complex atmospheric environments. The self-healing and replenishment from background energy reservoir and the generation of acoustic waves make filaments penetrate fog and clouds. The nonlinear effect of filaments can restrain the beam wander induced by turbulence. These unique properties make femtosecond laser filamentation applicable to remotely detecting atmospheric pollution, such as gases, aerosols, metals, and biological matter.

The lateral spatial distribution of fluorescence induced by the femtosecond laser filamentation is significance for measuring the parameters of laser intensity and plasma inside the filament, studying the physical process, and controlling the filament. It is a non-invasive and *in-situ* measurement method. The backward fluorescence distribution is useful for filament-based Lidar to promote the remote signal intensity and signal-to-noise ratio. Forward and backward air lasers are ideal light sources for remote sensing. Studying the far-field spatial distribution characteristics, such as the divergence angle and directivity, is important. This paper reviews the research progress of the spatial distribution of fluorescence induced by the femtosecond filamentation from lateral, backward, and forward spatial orientations.

Progress The laser polarization, repetition rate (Fig. 2), and the molecule alignment (Fig. 3) affect the lateral distribution of fluorescence, in addition to laser energy, chirp, and external focusing condition. Measuring the lateral distribution of fluorescence is a noninvasive and *in-situ* filament visualization method (Fig. 1); it measures the laser intensity (Fig. 5), plasma density, and

temperature (Fig. 6) inside the filament. It is a simpler and more sensitive method than measuring electrical conductivity, acoustic waves, and other pump-probe methods. Different physical phenomena have been discovered by measuring the lateral distribution, such as anti-correlated plasma density and THz pulse generation during two-color laser filamentation (Fig. 4). Controlling the filament is important for different filament-based applications, including controlling the laser intensity and plasma density inside the filament, controlling the spatial position and filament length, and organizing multiple filaments. Spatiotemporal phase modulation is used to enhance and elongate the filament (Fig. 8). Different spatial phase modulation methods, such as axicon, deformable mirror, phase plate, and beam ellipticity, are used to control the generation of multiple filaments (Fig. 9).

An amplified spontaneous emission inside the filament has been observed for different compositions, such as N_2, O, CN, OH, and NH (Fig. 10). Thus, the amplified spontaneous emission (ASE) phenomenon has gained considerable attention for air laser applications; furthermore, the backward spatial distribution and divergence angle are important remote sensing characteristics (Fig. 11). Backward N_2 lasers are generated with an energy conversion efficiency of 0.5% and a small divergence angle of 1.6 mrad (Fig. 11) by electron impact excitation. Different pump-probe methods have been proposed to generate forward air lasers, including self-generated harmonic waves, white light, and external probe beams. The forward spatial distribution is also analyzed with an annular profile (Fig. 15). The forward divergence angle is sensitive to the gas pressure and external focus length.

Conclusions and Prospects For filament characterization and control, understanding the physical process inside the filament, and generating air lasers, the spatial distribution of fluorescence induced by filaments is reviewed from lateral, backward, and forward spatial orientations. Challenges remain with the application of filamentation-based remote sensing. First, the physical mechanism of the interaction between filaments and molecules, dust, and aerosols, and the mechanism of fluorescence emissions still need to be studied. The mechanisms of gain and amplification inside the filament are also important. Second, the influence of complex atmosphere conditions on the spatial distribution is still unclear, including the turbulence, pressure, and temperature distribution in the atmosphere and atmosphere scattering and absorption. Third, controlling long-distance filaments and promoting remote signal intensity and the signal-to-noise detection ratio are also practically important.

Key words nonlinear optics; laser optics; femtosecond laser filamentation; remote atmosphere detection